nature nanotechnology
SUPPLEMENTARY INFORMATION
DOI: 10.1038/NNANO.2010.115

"Soft" Au, Pt, and Cu Contacts for Molecular Junctions via Surface Diffusion Mediated Deposition

Supplementary Information

Andrew P. Bonifas[1,2], Richard L. McCreery[2,3*]

[1] Department of Materials
Science and Engineering
The Ohio State University
2041 College Rd.
Columbus, OH, 43210

[2] National Institute for Nanotechnology
National Research Council of Canada
Canada, T6G 2G2

[3] Department of Chemistry
University of Alberta
Canada,T6G 2R3

*corresponding author
Tel.: 780-641-1760
Email: *richard.mccreery@ualberta.ca*

© 2010 Macmillan Publishers Limited. All rights reserved.

DOI: 10.1038/NNANO.2010.115

1. Introduction

This supplementary information provides additional details on the fabrication process, experimental conditions, and device characterization. The detailed information is included to provide additional support for stated conclusions in the main text and experimental details allowing external research groups to reproduce the reported results.

2. Fabrication

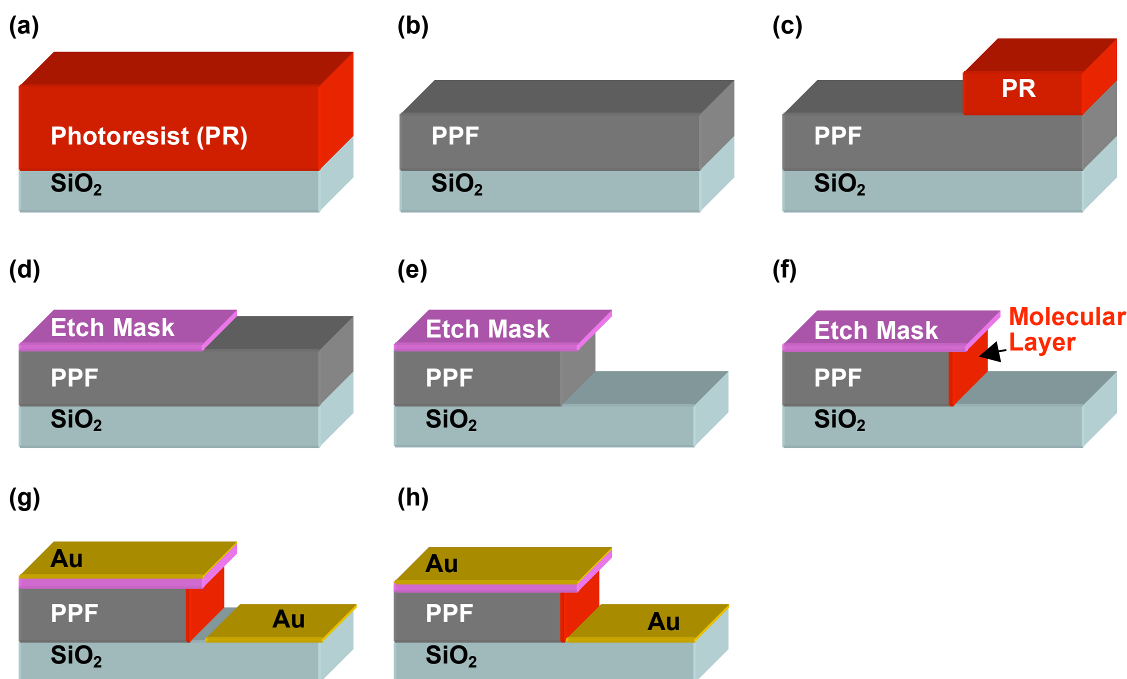

Figure S1 | Schematic of process flow chart: **(a)** Spin coat photoresist. **(b)** Pyrolysis of photoresist (PPF). **(c)** PPF patterned with photolithography. **(d)** Evaporation of Cr/SiO_2 RIE etch mask. **(e)** O_2 RIE of PPF. **(f)** Molecular layer formation. **(g)** Deposition of Au electrode. **(h)** Au surface diffusion mediates contact formation.

<u>PPF Fabrication</u>

Substrates consisted of either 1 mm thick fused silica microscope slides or p-Si with a 300 nm thick thermal SiO_2 insulation layer. Substrates were ultrasonically cleaned with sequential immersion in acetone, deionized water (TOC < 3 ppb), and isopropanol for 10 minutes. An Ar stream was used to dry the substrates. To form pyrolyzed photoresist films (PPF), the substrates were spin coated with photoresist AZ P4330-RS at 6000 rpm for 30 seconds, soft baked at 90°C for 10 minutes, and pyrolyzed in a tube furnace[1]. For the pyrolysis process, the temperature ramp rate with 8°C min^{-1} and held at 1000°C for 60 min in the presence of forming gas (5% hydrogen and 95% nitrogen) flowing at 100 cc/min. Metal tubing with brass fittings was used between the forming gas source and tube furnace to ensure the purity and H_2 content of the forming gas. The thickness of the PPF was between 700-800 nm as measured with a profilometer. For junctions fabricated

© 2010 Macmillan Publishers Limited. All rights reserved.

through direct metal evaporation, optical lithography was used to pattern the photoresist prior to pyrolysis resulting in PPF lines 1 mm x 18 mm.

PPF Side-Wall Fabrication

Conventional optical lithography (HPR504 photoresist) was used to pattern reactive ion etch (RIE) etch masks on the PPF layer through a lift-off technique. The etch masks were formed with electron beam evaporation of 3 nm Cr (adhesion layer) and 27 nm SiO_2 followed by lift-off in acetone. Chamber pressure during evaporation was less than 1 x 10^{-7} torr with deposition rates of 0.2 and 0.5 $Å \cdot s^{-1}$ for the Cr and SiO_2 layers respectively. Final dimensions of the Cr/SiO_2 etch masks were 1 mm x 18 mm. The PPF was etched with an O_2 RIE process to remove the PPF not protected by the etch mask. The RIE parameters were 200 watt RF plasma, O_2 pressure of 150 x 10^{-3} torr, and substrate DC bias of 360 V. The DC bias caused an anisotropic etch allowing for the formation of a near vertical sidewall. Uniform etching under the etch mask caused the etch mask to form the desired protective “overhang”. PPF was selected as the bottom contact because of our previous success with the diazonium attachment paradigm and the ability to create the sidewall geometry with a simple O_2 RIE. Methods to fabricate similar junction architectures using metals instead of PPF allowing additional molecular attachment paradigms are being investigated.

Molecular Layer Fabrication

For NAB and FL molecular layers, the corresponding diazonium salt was prepared from the precursors 4-4-Nitrophenylazoaniline (Aldrich, 90%) and 2-Aminofluorene (Aldrich, 98%), as previously described[2]. The molecular layers were attached to PPF through the electrochemical reduction of a 1.0 mM solution of the corresponding diazonium salt in acetonitrile (MeCN) containing 0.1 M n-tetrabutylammonium tetrafluoroborate ($TBABF_4$). For the NAB layer, four cyclic voltammetric scans were performed from 0.4 to -0.6 V versus Ag/Ag^+ at 200 $mV \cdot s^{-1}$. For the FL layer, one scan was performed from 0.4 to -0.8 V vs Ag/Ag^+ at 200 $mV \cdot s^{-1}$. Solutions were thoroughly degassed with Ar and blanketed with Ar during electrochemical deposition. After surface modification, the molecular layers were immediately rinsed in MeCN and dried in an Ar stream.

The diaminoalkane monolayers were prepared from the precursors 1,8-diaminoctane (TCI America, 95%), 1,10-diaminodecane (TCI America, 95%), and 1,12-diaminododecane (TCI America, 98%). Solutions of 1.0 mM diaminoalkane in MeCN containing 0.1 M $TBABF_4$ were stirred for 1 hour and then filtered through a 0.2 µm filter (Millipore Millex-FG). The monolayers were attached to the PPF through electrochemical oxidation at 0.8 V vs Ag/Ag^+ for 5 minutes. Solutions were degassed and blanketed with Ar during the oxidation process. The monolayers were rinsed with MeCN and dried in an Ar stream.

Thickness measurements of the molecular layer through atomic force microscopy or standard ellipsometry could not be directly performed because of the geometry of the PPF side-wall. Thicknesses of the molecular layers were estimated from molecular layers attached to a flat PPF surface under the same deposition conditions as the side-wall junctions. An AFM scratching technique was used to measure the molecular thickness, as previously described[3].

© 2010 Macmillan Publishers Limited. All rights reserved.

 DOI: 10.1038/NNANO.2010.115

Metal Contact Deposition

For surface diffusion mediated deposition (SDMD), Au, Cu, and Pt second contacts were deposited in a Johnson Ultravac load-lock electron beam evaporation system. The base pressure of the evaporation chamber was 5 x 10^{-8} torr allowing deposition pressures less than 2 x 10^{-7}. Since surface diffusivity depends on surface contaminants (e.g. O_2, H_2O), deposition pressure affects the diffusion length and junction contact area[4]. The 25 nm thick metallic contacts were evaporated through a shadow mask aligned perpendicular to the PPF lines with an evaporation rate of 0.5 Å·s^{-1}, as measured by a quartz crystal monitor (QCM). The deposition angle relative to the surface normal of the substrate was varied between 0 - 15°. An optical image of a junction fabricated with SDMD is shown in Fig. S2.

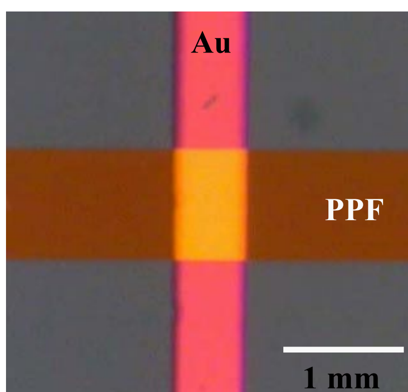

Figure S2 | Optical image of a PPF/NAB/Au junction fabricated with SDMD. Junction is located at the top intersection of the PPF and Au lines.

The Johnson Ultravac system has a metal source – junction (throw) distance of 45 cm and a metal source radius of about 8 mm. Since evaporation does not occur from a single point on the metal source, the reported deposition angles have a range of ± 0.5°. This angle range is sufficiently small to distinguish between deposition angles of 0°, 5°, and 15°. It should be noted that the electron beam size was minimized during evaporation resulting in a melted source radius of about 2 mm.

For direct metal evaporation, Au, Cu, and Pt top contacts were deposited through a shadow mask in a K.J. Lesker PVD75 electron beam evaporation system. For all metallic contacts, 10 nm was deposited with a chamber pressure less than 5 x 10^{-6} torr at 0.2 Å·s^{-1}. For the Cu junctions, an additional 15 nm of Au was deposited on top of the Cu contact to prevent oxidation of the Cu.

© 2010 Macmillan Publishers Limited. All rights reserved.

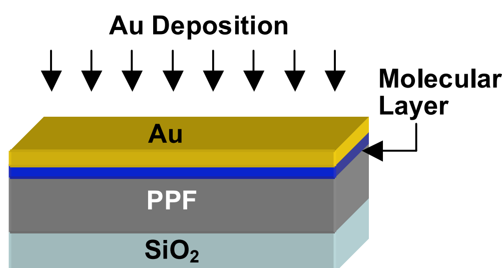

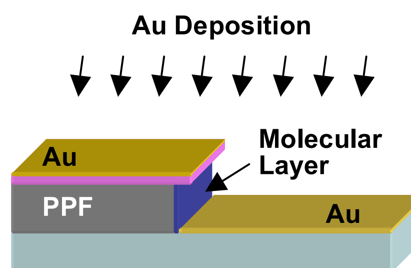

Figure S3 | Schematic representation of molecular junctions fabricated through direct evaporation and SDMD techniques.

3. Characterization

Spectroscopy

Raman spectroscopy was used to determine if structural damage occurred to a NAB molecular layer during direct Au deposition. The spectra were measured on a flat PPF surface modified with a NAB molecular layer before and after deposition. A custom built spectrometer[5] consisting of an Ar ion laser (514.5 nm), a 50 mm f/1.8 lens, a holographic reflection grating (2000 grove/mm), and an Andor back-thinned CCD detector cooled to -80° C was used to acquire the spectra. The incident laser power was 19 mW with a spot diameter of 17 µm. The integration time was 30 seconds and the Raman shift was calibrated with naphthalene. Fig. S4 shows the PPF/NAB Raman spectra before and after direct evaporation of 10 nm of Au. Comparison of the spectra confirms that observable changes in the Raman spectrum are absent during metal deposition, providing strong evidence that the NAB molecular layer is not damaged during direct Au deposition. The decrease in Raman intensity after Au deposition was caused by the partial transparency of the Au contact. This result is consistent with our previous reports for the deposition of Au on our molecular layers[6]. Given the absence of apparent damage by Au deposition, the shorted devices resulting from direct Au deposition are likely caused by Au penetration between molecular units or packing defects in the molecular layer.

© 2010 Macmillan Publishers Limited. All rights reserved.

DOI: 10.1038/NNANO.2010.115

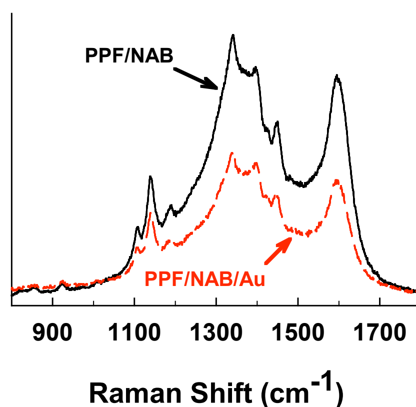

Figure S4 | Raman spectra of a PPF/NAB layer before (black) and after (red) evaporation of 10 nm Au indicating structural damage to the molecular layer does not occur. The spectra were collected with a signal integration time of 30 s.

SEM and TEM

SEM images were taken with a Hitachi S4800. Cross-sectional samples were made by cleaving the Si/SiO_2 substrate across the molecular junction. Low acceleration voltages and beam currents (5kV, 5μA) allowed sufficient resolution while minimizing sample charging. TEM lamellae of the molecular junctions were milled with a Zeiss Nvision focused ion beam (FIB). Prior to milling, the molecular junctions were coated with several micrometers of carbon to minimize sputtering and redeposition during the milling process. For the FIB process, 30 keV Ga ions were used to mill the lamellae to thicknesses below 100 nm and 5 keV Ga ions were used for final polishing. A Joel 2200FS TEM operating at 200 kV was used to acquire bright field images and diffraction patterns. The molecular layer was not resolved from the PPF surface.

SEM micrographs of PPF/NAB/Au and PPF/NAB/Cr junctions are shown in Fig. S5. For both junctions, 25 nm of the metal contact was deposited at 5° relative to the surface normal. For the PPF/NAB/Au junction, surface diffusion on the SiO_2 surface was sufficient to allow the Au to diffuse onto the PPF/NAB sidewall. For the PPF/NAB/Cr junction, the deposited Cr layer did not reach the PPF/NAB sidewall. The shorter Cr diffusion length could have been caused by a higher diffusion activation energy or parasitic interaction with surface contaminants (e.g. H_2O, O_2) on the SiO_2 substrate[7]. Performing SDMD at different deposition pressures could be used to provide additional insight into this phenomenon.

© 2010 Macmillan Publishers Limited. All rights reserved.

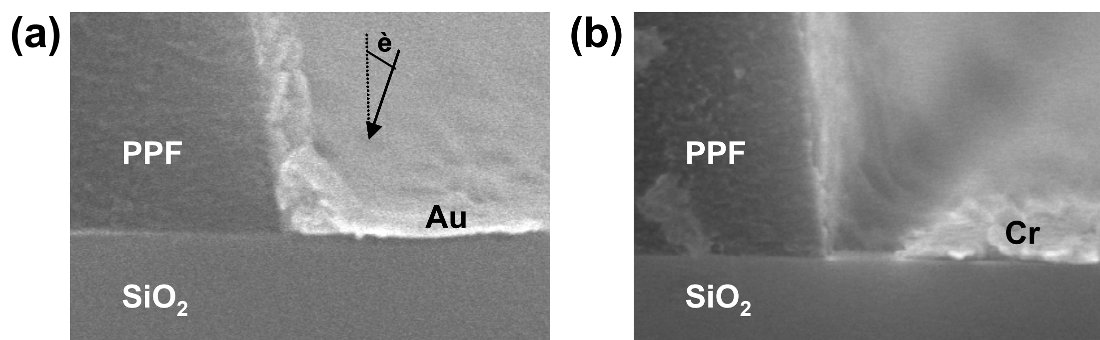

Figure S5 | Secondary electron SEM micrographs of NAB junctions. Deposition of **(a)** 25 nm Au has adequate surface diffusion to reach the PPF/NAB surface. **(b)** 25 nm Cr does not reach the PPF/NAB surface.

To calculate the current-density, the diffusion length of the metal contact onto the molecular layer was measured. For each test chip, which contained 6 to 9 individual junctions, we cleaved the substrate perpendicular to the PPF contacts, leaving a cross section of the junction. The diffusion length onto the molecular layer was measured at two locations on the test chip, showing variability less than 20% between measurements. Backscattered SEM images were used to determine the diffusion length onto the molecules. Similar to TEM, backscattered SEM images provide strong atomic number contrast. TEM images of a PPF/NAB/Au junction were used to confirm the calibration of the SEM images. The areas of the final junctions were between 0.25 um^2 (FL) and 1.5 um^2 (NAB), depending on the molecular layer type. For each molecular layer type the junction area was consistent between samples.

Electronic Characterization

Electronic characterization was performed with a three probe format allowing for the correction of resistance errors associated with the PPF contact. Junction architecture does not allow an additional fourth contact probe to correct for resistance associated with the metal contacts. Since the measured currents were on the order of several to tens of microamperes, IR error is expected to be negligible. Current density – voltage (J-V) curves were measured using a custom setup of a National Instruments 6110 data acquisition board and a Stanford Research Systems 570 current amplifier programmed with Labview software. The junction voltage was scanned between 0 to ±1 V with a scan rate of 10 $V \cdot s^{-1}$. Current amplification and analog filtering parameters were carefully selected to reduce noise without affecting the J-V response. **For all electronic measurements, the stated voltage is the PPF contact relative to the metallic contact.**

Changing the deposition angle relative to the substrate surface normal resulted in different measured resistances of the fabricated junctions. The measured resistances at 0.8 V for PPF/Au, PPF/NAB/Au, and PPF/NAB/Cr junctions as a function of the SDMD deposition angle are shown in Table S1. For junctions absent of a molecular layer, deposition at 0° resulted in an open circuit between the PPF and Au contacts ($R > 10$ GΩ). Compared to 0°, deposition at 5° caused the Au atoms to land about 50-70 nm closer to the PPF side-wall resulting in electronic contact between the PPF and Au contacts. At 15°, the depositing Au atoms are directly incident on the PPF side-wall, thus creating electronic contact. For the deposition of Cr at 0° and 5°, the deposited Cr layers

© 2010 Macmillan Publishers Limited. All rights reserved.

 DOI: 10.1038/NNANO.2010.115

did not reach the molecular layer, resulting in an open circuit. Unlike Au deposition at 5°, Cr surface diffusion was insufficient to reach the PPF side-wall. Cr deposition at 15° resulted in electronic contact, showing that the deposited Cr layer was conductive. For junctions consisting of a NAB molecular layer, deposition at 5° resulted in Au diffusion onto the NAB layer, and produced the J-V behavior of Fig. 3a in the main text. Deposition at 15° resulted in shorted junctions with a similar J-V response to the directly evaporated Au junctions.

	è = 0°	è = 5°	è = 15°
PPF/Au	> 10GÙ	< 100Ù	< 100Ù
PPF/Cr	> 10GÙ	> 10GÙ	< 100Ù
PPF/NAB/Au	> 10GÙ	~ 10MÙ	< 100Ù

Table S1 | Junction resistances at 0.8 V for SDMD junctions as a function of the deposition angle (θ) relative to the surface normal.

With the SDMD technique, NAB junctions were successfully fabricated with Cu, Au, and Pt allowing direct comparison between several contacts, a comparison not possible with direct evaporation. A powerful comparison metric is the asymmetry ratio between the current density at ±1 V. Comparison of the asymmetry ratio has the advantage of removing errors associated with contact area variation between junctions. Also, current asymmetry through a molecular junction should directly depend on the work functions (φ) of the contacts. As shown in Fig. 4c and Table S2, the asymmetry ratio (J_{pos}/J_{neg}) of the PPF/NAB junctions varied with changes in the metal contact. The p-values for a statistical test of the differences between the asymmetry ratios for the three top contacts indicate that the values differ to a very high degree of certainty. The asymmetry ratio trend is consistent with that expected from the work function of the contact, with an increase in the contact work function ($\varphi_{Cu} < \varphi_{Au} < \varphi_{Pt}$) resulting in a lower asymmetry ratio (J_{pos}/J_{neg}).

	NAB/Cu	**NAB/Au**	**NAB/Pt**
J_{pos} [1V]	0.66	1.69	1.33
J_{neg} [-1V]	-0.48	-1.99	-2.85
J_{pos} / J_{neg}	1.38	0.85	0.47
H_o: $J_{pos} = J_{neg}$	$p = 9\times10^{-6}$	$p = 7\times10^{-8}$	$p = 5\times10^{-6}$

Table S2 | Current density asymmetry at ±1 V for junctions with three different metal contacts. Data represents the average data of at least 5 junctions on one test chip. The asymmetry ratios are statistically different as represented by the rejection of the null hypothesis (H_o) and correlate with the work function of the contacts.

© 2010 Macmillan Publishers Limited. All rights reserved.

Low temperature electronic characterization was carried out with a Janis ST-500 cryogenic probe station with a Scientific Instruments temperature controller. The junction chamber was pumped to 2 x 10^{-6} torr before collecting J-V curves. The temperature was varied between 300-77 K, acquiring J-V curves every 0.001 K^{-1}. As mentioned above, the contact resistance of the metallic contact was not corrected during the measurements.

In-situ electronic monitoring during the SDMD process was achieved via a high vacuum electrical pass-through on the chamber of the evaporation system. Conducting Ag epoxy was used to connect lead wires to the PPF and to the Si/SiO_2 substrate. During Au deposition, the forming Au contact was positioned with a shadow mask to contact the attached lead wire on the substrate. A schematic of the in-situ setup is shown in Fig. S6.

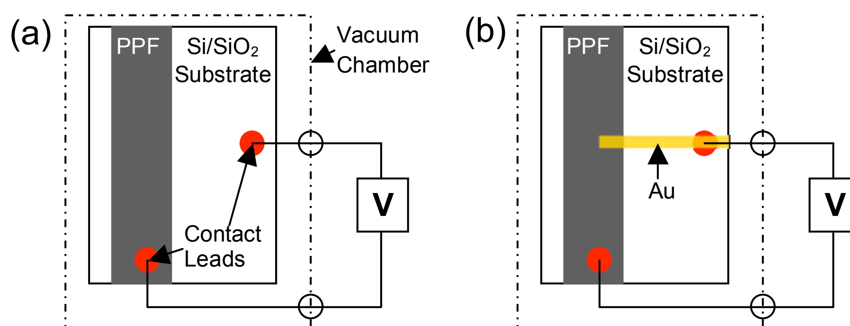

Figure S6 | Schematic of an in-situ monitored SDMD junction. **(a)** Contact leads are connected to the PPF and substrate. **(b)** Au deposition on top of substrate lead permits in-situ electronic measurements.

Current-voltage (I-V) curves of a forming PPF/NAB/Au junction are shown in Fig. S7. The current was measured at 0.2, 0.4 and 0.8 V after each 2 nm increment of Au deposition. To lessen possible effects of applied electric fields during junction formation, I-V measurement time was keep to a minimum. Fig. S7a shows the normalized current (relative to the current measured at +1 V) for several thickness of the Au contact. Similar shape of the I-V responses indicates consistent contact formation during the diffusion deposition process. Fig. S7b shows the current as a function of Au thickness at 0.2, 0.5 and 0.8 V. A conduction threshold thickness of 10 nm was observed which is higher than the percolation (conduction) threshold of 8 nm for an Au layer under the same deposition conditions. The difference of 2 nm could be attributed to the migrating edge of the Au layer not yet reaching the molecular layer although the deposited Au layer is conductive.

© 2010 Macmillan Publishers Limited. All rights reserved.

 DOI: 10.1038/NNANO.2010.115

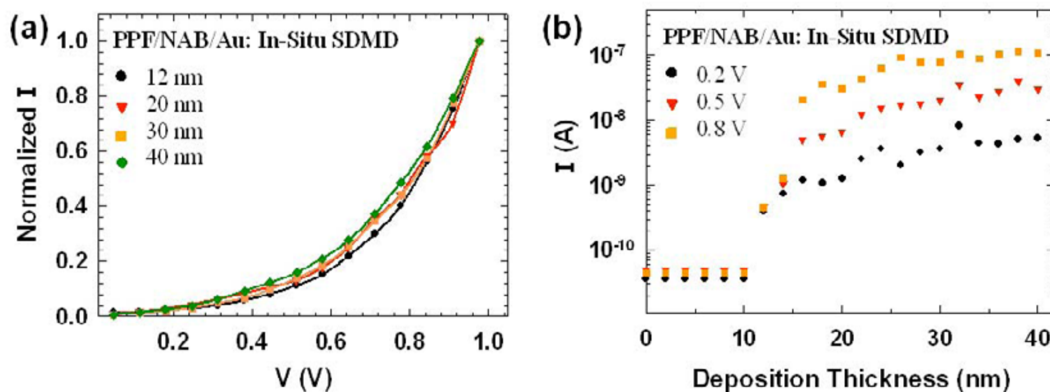

Figure S7 | In-situ monitoring of a forming SDMD PPF/NAB/Au junction during Au deposition. **(a)** Normalized I-V curve for several Au thicknesses. **(b)** Current as a function of the Au thickness at several voltages.

The J-V characteristics for the diaminoalkane monolayers is consistent with off-resonance tunneling through the molecular layer characterized by an exponential decrease in current-density with an increase in monolayer thickness. Fig. S8 show the change in current density at 0.5 V versus the length of diaminoalkane molecules. The decay constant β was calculated to be 1.1 per carbon atom (0.88 $Å^{-1}$) which compares well to reported β in alkanes[8,9].

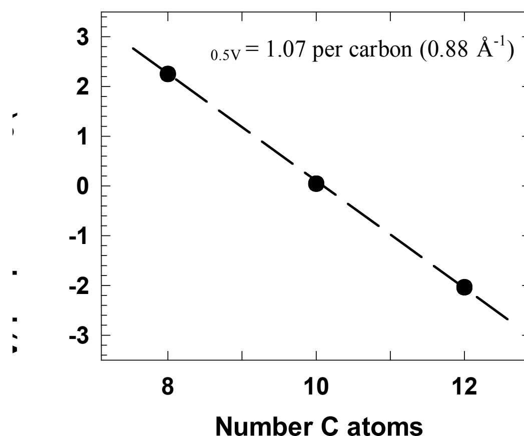

Figure S8 | Calculation of the decay constant β for the diaminoalkane monolayer junctions at 0.5 V. The dashed line represents the linear regression fit for C_8, C_{10}, C_{12} junctions. Plotted points are the average of at least five junctions for each monolayer length.

© 2010 Macmillan Publishers Limited. All rights reserved.

4. References

1. Ranganathan, S. & McCreery, R.L. Electroanalytical performance of carbon films with near-atomic flatness. *Anal. Chem.* **73**, 893-900 (2001).
2. Dunker, M.F.W., Starkey, E.B. & Jenkins, G.L. The preparation of some organic mercurials from diazonium borofluorides. *J. Am. Chem. Soc.* **58**, 2308-2309 (1936).
3. Anariba, F., DuVall, S.H. & McCreery, R.L. Mono- and multilayer formation by diazonium reduction on carbon surfaces monitored with atomic force microscopy "scratching". *Anal. Chem.* **75**, 3837-3844 (2003).
4. Abelmann, L. & Lodder, C. Oblique evaporation and surface diffusion. *Thin Solid Films* **305**, 1-21 (1997).
5. Ramsey, J., Ranganathan, S., McCreery, R.L. & Zhao, J. Performance comparisons of conventional and line-focused surface Raman spectrometers. *Appl. Spectrosc.* **55**, 767-773 (2001).
6. Mahmoud, A.M., Bergren, A.J. & McCreery, R.L. Derivatization of Optically Transparent Materials with Diazonium Reagents for Spectroscopy of Buried Interfaces. *Anal. Chem.* **81**, 6972-6980 (2009).
7. Racz, Z. & Seabaugh, A. Characterization and control of unconfined lateral diffusion under stencil masks. *J. Vac. Sci. Technol. B* **25**, 857-861 (2007).
8. Engelkes, V.B., Beebe, J.M. & Frisbie, C.D. Length-dependent transport in molecular junctions based on SAMs of alkanethiols and alkanedithiols: Effect of metal work function and applied bias on tunneling efficiency and contact resistance. *J. Am. Chem. Soc.* **126**, 14287-14296 (2004).
9. Holmlin, R.E. et al. Electron transport through thin organic films in metal-insulator-metal junctions based on self-assembled monolayers. *J. Am. Chem. Soc.* **123**, 5075-5085 (2001).

© 2010 Macmillan Publishers Limited. All rights reserved.